

The outer profile of dark matter halos: an analytical approach

Xun Shi [★]

Max-Planck-Institut für Astrophysik, Karl-Schwarzschild-Straße 1, D-85740 Garching bei München, Germany

14 June 2016

ABSTRACT

A steepening feature in the outer density profiles of dark matter halos indicating the splashback radius has drawn much attention recently. Possible observational detections have even been made for galaxy clusters. Theoretically, Adhikari et al. have estimated the location of the splashback radius by computing the secondary infall trajectory of a dark matter shell through a growing dark matter halo with an NFW profile. However, since they imposed a shape of the halo profile rather than computing it consistently from the trajectories of the dark matter shells, they could not provide the full shape of the dark matter profile around the splashback radius. We improve on this by extending the self-similar spherical collapse model of Fillmore & Goldreich to a Λ CDM universe. This allows us to compute the dark matter halo profile and the trajectories simultaneously from the mass accretion history. Our results on the splashback location agree qualitatively with Adhikari et al. but with small quantitative differences at large mass accretion rates. We present new fitting formulae for the splashback radius R_{sp} in various forms, including the ratios of $R_{\text{sp}}/R_{200\text{c}}$ and $R_{\text{sp}}/R_{200\text{m}}$. Numerical simulations have made the puzzling discovery that the splashback radius scales well with $R_{200\text{m}}$ but not with $R_{200\text{c}}$. We trace the origin of this to be the correlated increase of Ω_{m} and the average halo mass accretion rate with an increasing redshift.

Key words: cosmology: theory – dark matter – methods: analytical – galaxies: clusters: general

1 INTRODUCTION

Recent numerical simulations (Diemer & Kravtsov 2014) have noticed a sharp steepening in the outer density profiles of dark matter halos, which seems to offer a physical boundary of dark matter halos (More, Diemer & Kravtsov 2015). Although this steepening feature lies in a low density region in the outskirts of a dark matter halo and thus hard to detect, potential observational evidences have been found by studying the projected number density profiles of galaxies around galaxy clusters (Patej & Loeb 2015; More et al. 2016).

Physically, this steepening feature has been identified with the ‘splashback’ of recently accreted dark matter i.e. piling up of dark matter near the first apocenter of its orbit through the halo (Diemer & Kravtsov 2014). With this physical picture, Adhikari, Dalal & Chamberlain (2014) theoretically estimated the radial position of the splashback R_{sp} . They computed R_{sp} by tracing the trajectory of a dark matter shell accreted onto a dark matter halo and then going through it, and described the dark matter halo with an NFW profile (Navarro, Frenk & White 1996, 1997) with its mass increasing with time. They found good agreement of the predicted splashback radius and the steepening position from the stacked halos in the Diemer & Kravtsov (2014) simulations. However, one weakness

of their method is that the imposed NFW shape of the halo profile and the trajectories of the dark matter shells are not fully consistent with each other. Although this may not affect their estimation for R_{sp} to a large extent, it prevents them from giving the full shape of the dark matter profile around the splashback radius.

In fact, the steepening feature at halo outskirts has been known for long time in the self-similar spherical collapse model (Fillmore & Goldreich 1984; Bertschinger 1985; Lithwick & Dalal 2011) as associated with the outmost caustic. In contrast, the caustics in dark matter halos had not been noticed in three-dimensional numerical simulations due to resolution limits until lately when special techniques were applied (Vogelsberger et al. 2009; Hahn & Angulo 2016). As the outer profiles of dark matter halos are primarily determined by the recent mass accretion, and the matter there has relatively little participation in the relaxation processes which require numerical simulations to capture, the self-similar spherical collapse model is actually rather adequate in describing the outer profile of dark matter halos. Another merit of the self-similar spherical collapse model is that the halo profile and the trajectories of the dark matter shells are treated consistently with iterations of computing one from the other.

Thus we use the self-similar spherical collapse model to compute the outer profiles of dark matter halos. One obstacle remains still, that the self-similarity is strictly valid only in a universe with no characteristic scales, e.g. an Einstein de-Sitter (EdS) universe

[★] E-mail: xun@mpa-garching.mpg.de

($\Omega_m = 1$) as considered in previous studies (Fillmore & Goldreich 1984; Bertschinger 1985; Lithwick & Dalal 2011). Here we extend the model to a Λ CDM universe by relaxing the self-similarity ansatz while keeping its feature of computing trajectories and halo profile in a consistent manner.

The rest of the paper is organised as follows. In Sect. 2 we describe the detailed procedures of our computation and the resulting mass and density profiles of dark matter halos. Then we derive analytical interpretations of the results, and provide fitting formulae in Sect. 3, summarise our findings and conclude in Sec. 4. We present the minimalistic dimensionless form of spherical collapse in a Λ CDM universe in Appendix. A, which scales out the cosmology dependence in the variables and has thus greatly reduced our computational cost. With this form, many relations among the variables as well as the dark matter density profile in the single stream regime of spherical collapse can be expressed in simple analytical forms, which we show in Appendices. A1 and A2. Finally, in Appendix. B we present a physical estimation of the splashback radius in an EdS universe.

2 MASS AND DENSITY PROFILES FROM PROFILE-TRAJECTORY ITERATION

2.1 Methods

We look for the asymptotic profile of dark matter halos as a function of their mass accretion rate and the background cosmology. For simplicity, we restrict ourselves to a flat Λ CDM universe with $\Omega_m + \Omega_\Lambda = 1$, and study the case of power law mass growth $M_{\text{vir}} \propto a^s$ where a is the cosmic scale factor. Thus, the two basic parameters in our study are the mass accretion rate s and the dimensionless matter density of the universe $\Omega_m(a)$.

Power law mass growth is typical for dark matter halos in our Universe at low redshifts (e.g. Correa et al. 2015). The typical mass growth rate is $s \lesssim 1$ for galaxy mass halos today, and increases with redshift and halo mass. Following Adhikari, Dalal & Chamberlain (2014), we use the mass enclosed by the shell that has collapsed to half of its turn-around radius $M_{\text{hrt}}a$ under no shell-crossing as a proxy for the virial mass M_{vir} of the halo. This matches the early definition of virial radius in a spherical collapse model (Lacey & Cole 1993). With this definition, the relative sizes of dark matter shells are specified by their dimensionless trajectories (Appendix. A) when the mass growth history is given.

In a multi-stream region such as a dark matter halo, the dark matter trajectory depends on the halo mass profile and vice versa, thus an iteration is needed in computing the two. Under strict self-similarity, the trajectory of one dark matter shell also represents the locations of all dark matter shells in a snapshot, and thus within each iteration, only one integration of orbit is needed. In a Λ CDM universe, we lose such simplification, and need to compute the trajectories of the dark matter shells accreted at different times simultaneously. To reduce this computational cost, we simplify the spherical collapse equations to a minimalistic dimensionless form (Appendix. A). The loss of strict self-similarity also means that the mass profile is time dependent. Luckily, in our Universe where the dark energy is still not entirely dominating, this time dependence is mild and slow - on the timescale of change of $\Omega_m(a)$, see Fig. 2. Over a dynamical time which is shorter compared to this timescale, the mass profile can be approximated as being constant.

Therefore, we parametrize the mass in the multi-stream region as $M(R) = M_{\text{hrt}}(a)f(R/R_{\text{hrt}})$, with an initial choice of $f_0(x) = x$.

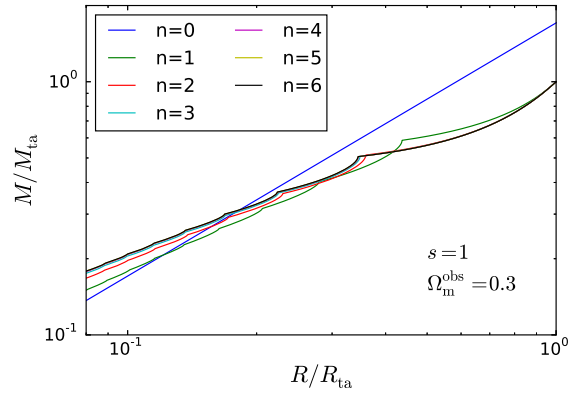


Figure 1. Mass profile converges quickly with the number of iteration n . The plotted mass is scaled to M_{ta} , the mass within the turn-around radius R_{ta} .

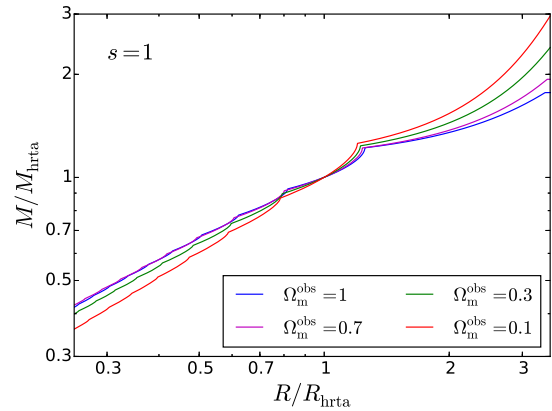


Figure 2. Dependence of the halo mass profile on Ω_m^{obs} .

Then we compute the trajectories of the shells till the time the halo is observed, which is specified by the value of Ω_m^{obs} . Using the trajectories we update the form of mass profile to $f_1(x)$, compute the trajectories again, and iterate. The mass profile and trajectories converge quickly with the number of iterations n (Fig. 1). As shown by Fig. 2, the shape of the mass profile scaled to R_{hrt} is indeed only slightly time-dependent, even over a long time range indicated by the change of the matter content of the universe Ω_m^{obs} .

2.2 Results

The converged mass profiles, the density profiles derived from them, and their dependencies on Ω_m^{obs} and the mass accretion rate s are shown in Fig. 3. We find three features that characterise the general shapes of the mass and density profiles: a power-law inner slope, the splashback feature, and a smooth profile outside the splashback radius where the matter is still on its infall towards the halo. The other caustics in the density profiles (middle column of Fig. 3) are hardly observable after smoothing (right column of Fig. 3) which in reality would be caused by e.g. asphericity of the halo and instability to perturbations (Henriksen & Widrow 1999).

The power-law inner mass profile $M \propto R^\gamma$ has been studied by Fillmore & Goldreich (1984) in an EdS universe. There, the mass accretion rate is related to the logarithmic slope ϵ of the initial

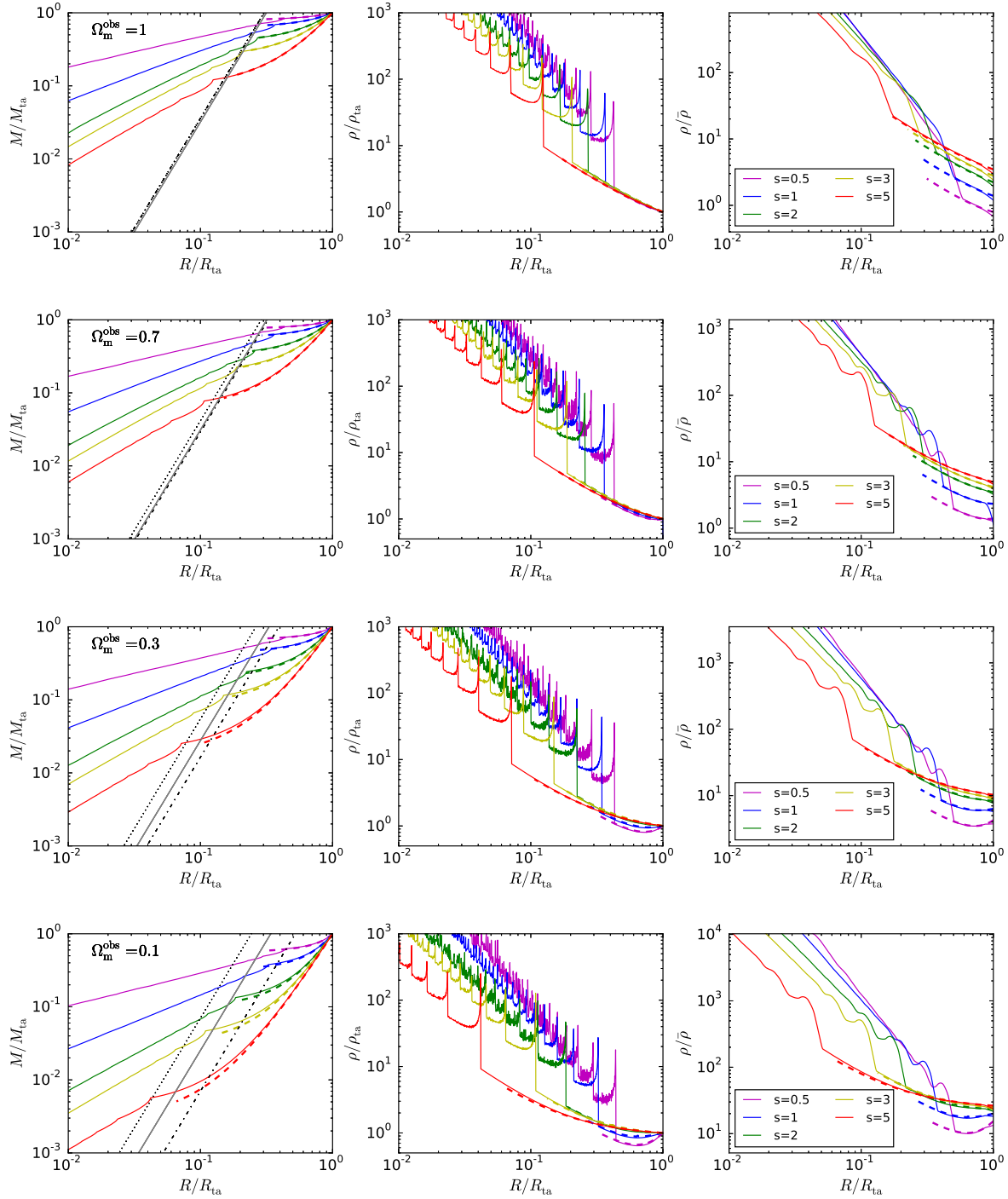


Figure 3. Profiles of mass (left), density (middle) and smoothed density (right) for different values of Ω_m^{obs} (different rows) and different mass accretion rate s (colored lines in each panel) from the mass profile - trajectory iterations. The color dashed lines show the analytical mass and density profile given by Eq. (A17). The black dotted and dashed lines in the left column mark the locations of $\Delta_c = 200$ and $\Delta_m = 200$ respectively, and intersection between the gray solid line and the color lines show the locations of the virial radius.

mass perturbation $\delta M_i/M_i \propto M_i^{-\epsilon}$ with $s = 1/\epsilon$. In terms of s , the Fillmore & Goldreich (1984) result reads

$$\Upsilon = \begin{cases} 3s/(s+3) & \text{if } s \leq 3/2 \\ 1 & \text{if } s \geq 3/2. \end{cases} \quad (1)$$

We reproduce this inner slope dependence on s not only when

$\Omega_m^{\text{obs}} = 1$, but also for other Ω_m^{obs} values (first column of Fig. 3). This is expected since the inner profiles are composed primarily of shells collapsed at early times when dark matter dominates the energy content of the universe. Admittedly, in the very inner regions of dark matter halos, especially within the scale radius of an NFW profile, the dynamics of dark matter particles is heavily influenced

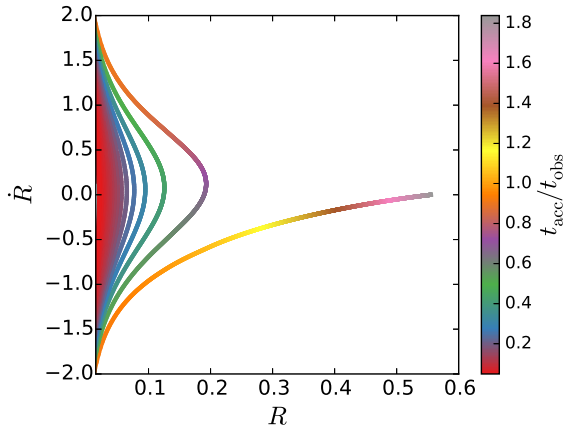


Figure 4. Instantaneous phase space locations of the shells at the time of observation when $\Omega_m^{\text{obs}} = 0.3$. The color coding shows the time when the shells are accreted by the halo t_{acc} compared to the time of observation t_{obs} . Here, the accretion rate $s = 1$.

by relaxation mechanisms including the radial orbit instability (e.g. Merritt & Aguilar 1985; MacMillan, Widrow & Henriksen 2006; Vogelsberger, Mohayaee & White 2011), and the angular momentum of the particles cannot be neglected. The one-dimensional accretion model we use naturally cannot reproduce the true dark matter profiles in these regions. However, as the dynamical time in the central region is very short, the inner profile should not have much influence on the dark matter dynamics and profiles in the outer regions.

The sharp jump in the density profile at the splashback radius is evident in all cases, and the amplitude of the density jump for the un-smoothed density profile always lies around a factor of 4 to 5. This can be understood considering that the splashback radius separates the regions with one and three dark matter streams (Fig. 4), and that the earlier accreted matter is denser than the matter currently being accreted. What depends on the accretion rate and the cosmology is the location of the splashback radius, as has been discovered by previous studies (Adhikari, Dalal & Chamberlain 2014; Diemer & Kravtsov 2014). As shown by Fig. 3, the ratio of the splashback radius and the turn-around radius decreases with the accretion rate s . For low accretion rates, the ratio is approximately independent of Ω_m^{obs} , whereas the decreasing with s at high accretion rate is more significant for a universe with low matter content. We investigate the locations of the splashback radius in more details in Sect. 3.1, where we provide explanations to these behaviors.

Outside the splashback radius and within the turn-around radius, the matter is still on its initial infall onto the halo. The dark matter density profiles in this regime (color solid lines in the middle and right columns of Fig. 3 outside the splashback radius) represent the correlated matter around the halo, or the so-called 2-halo term. Instead of modeling the profiles in this region in an averaged sense from the matter power spectrum, we can describe them using the spherical collapse model to take account of the dependence on the accretion rate of the individual halos. Indeed, the numerically integrated profiles match well with the single-stream analytical profiles (color dashed lines) given in Appendix. A2.

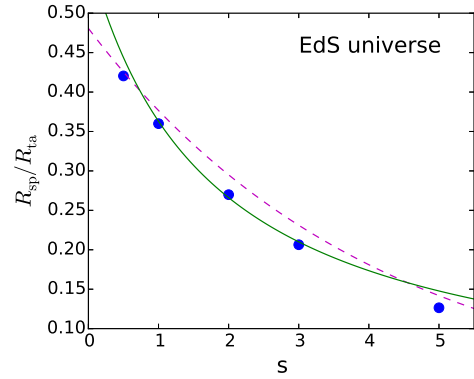


Figure 5. The ratio of splashback radius and the turnaround radius at the time of observation in an EdS universe as a function of accretion rate s . The analytical formula given in Eq. (2) for $s \leq 3/2$ (magenta dash line) and $s \geq 3/2$ (green solid line) agree well with the numerical results (blue circles).

3 ANALYTICAL INTERPRETATIONS AND FITTING FORMULA

3.1 The splashback radius

After turning around, dark matter shells begin to oscillate in the gravitational potential of the dark matter halo. Approximating the mass profiles by their inner power law shape, $M = (R/R_{\text{ta}})^{\Upsilon} M_{\text{ta}}$ with Υ given by Eq. (1), one can see that the gravitational potential of the dark matter halo in a Eulerian coordinates grows with time when the accretion rate $s > 3/2$ while stays approximately constant when $s \leq 3/2$.

We study the location of the splashback radius by tracing the dynamics of the oscillating orbits in these two regimes. In an EdS universe, approximate analytical solutions to the dynamical equation can be obtained as (Appendix. B)

$$\frac{R_{\text{sp}}}{R_{\text{ta}}} \approx \begin{cases} 3^{-2/3-2s/9} & \text{when } s \leq 3/2, \\ \left[1 + 4(4s/9 + 1/3)/\sqrt{\pi}\right]^{-1} & \text{when } s \geq 3/2, \end{cases} \quad (2)$$

which well-describes the smaller $R_{\text{sp}}/R_{\text{ta}}$ ratio for the range of mass accretion rates we have tested (Fig. 5). Different approximations are taken for the two regimes $s \leq 3/2$ and $s \geq 3/2$ and they lead to slightly different $R_{\text{sp}}/R_{\text{ta}}$ values at $s = 3/2$ (see Appendix. B for details).

In a Λ CDM universe, the growth of the turn-around radius with time is more significant at a certain mass accretion rate compared to the case of an EdS universe, due to the additional expansion caused by the dark energy. This explains the smaller $R_{\text{sp}}/R_{\text{ta}}$ ratio when Ω_m^{obs} is smaller (Fig. 3). This effect is more pronounced for a larger mass accretion rate. In the limit of small accretion rate $s \rightarrow 0$, the $R_{\text{sp}}/R_{\text{ta}}$ ratio stays approximately invariant with the change of the cosmological background. As evident in Fig. 3, for the lowest accretion rate we sampled, $s = 0.5$, the position of the splashback radius already approaches the asymptotic value of $R_{\text{sp}}/R_{\text{ta}} = 3^{-2/3} \lesssim 0.5$.

3.2 Time when the splashback matter was accreted

Since the actual mass accretion rate of a dark matter halo changes with time, how to match the mass accretion rates in simulations to the idealised accretion rate s defined from a power-law mass accretion history is non-trivial. Current numerical studies

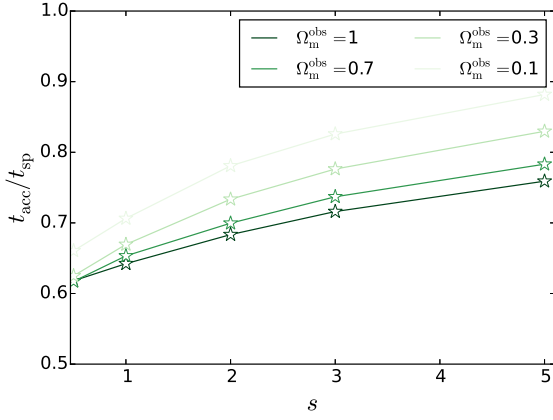


Figure 6. The time when the matter at the splashback radius was accreted t_{acc} compared to the time it is observed at the splashback radius t_{sp} .

commonly apply $\Gamma = \Delta \log M / \Delta \log a$ over a fixed cosmic scale factor interval to the simulated halos (e.g. Diemer & Kravtsov 2014; Adhikari, Dalal & Chamberlain 2014; Lau et al. 2015), and $\Gamma \approx s$ is often assumed when comparing to analytical results. This simplified assumption is possibly the biggest limitation to the precision of the comparison between the analytical predictions and the numerical results. To improve on this, it is useful to know the time when the splashback matter was accreted.

Regarding the orbit of a dark matter shell as an oscillation starting from the beginning of its expansion, the turn-around happens at phase $1/4$ of the first oscillation, accretion onto the halo happens at around phase $1/2$, and splashback happens at phase $3/4$. Thus, the age of the universe at which the matter currently at the splashback radius was accreted on to the halo t_{acc} ¹ should be close to $(1/2)/(3/4) = 2/3$ of the current age t_{sp} at low accretion rates where the halo potential is roughly constant with time. This rough estimate is supported by the results from numerical integration shown in Figs. 4 and 6. In detail, the ratio of $t_{\text{acc}}/t_{\text{sp}}$ increases with increasing accretion rate and decreasing matter density of the universe. This means, for example, that the splashback matter at redshift zero in a flat universe with $\Omega_{\text{m}0} = 0.3$ was accreted at approximately redshift $z \approx 0.4$ for an accretion rate $s = 1$ and $z \approx 0.2$ for an accretion rate $s = 5$. This gives a hint on how to choose the redshift range to average the mass accretion rate measured in simulations for a comparison study.

3.3 Fitting formulae and comparison to previous studies

Since we have computed the halo mass profile and the splashback location consistently, we can study the splashback location with respect to the commonly used radii defined from the halo mass profile, e.g. R_{200c} , R_{200m} and R_{vir} . Here we provide fitting formulae for the locations of the splashback radius in terms of these radii as functions of the mass accretion rate s and the matter content of the universe $\Omega_{\text{m}}^{\text{obs}}$.

$$\frac{R_{\text{sp}}}{R_{200c}} = \text{Exp} \left[(-0.22 + 0.03s) \ln \Omega_{\text{m}}^{\text{obs}} + 0.54 - 0.15s \right], \quad (3)$$

¹ Here, we use t_{trta} , the time when the shell collapses to half its turn-around radius, to define the ‘accretion time’ t_{acc} .

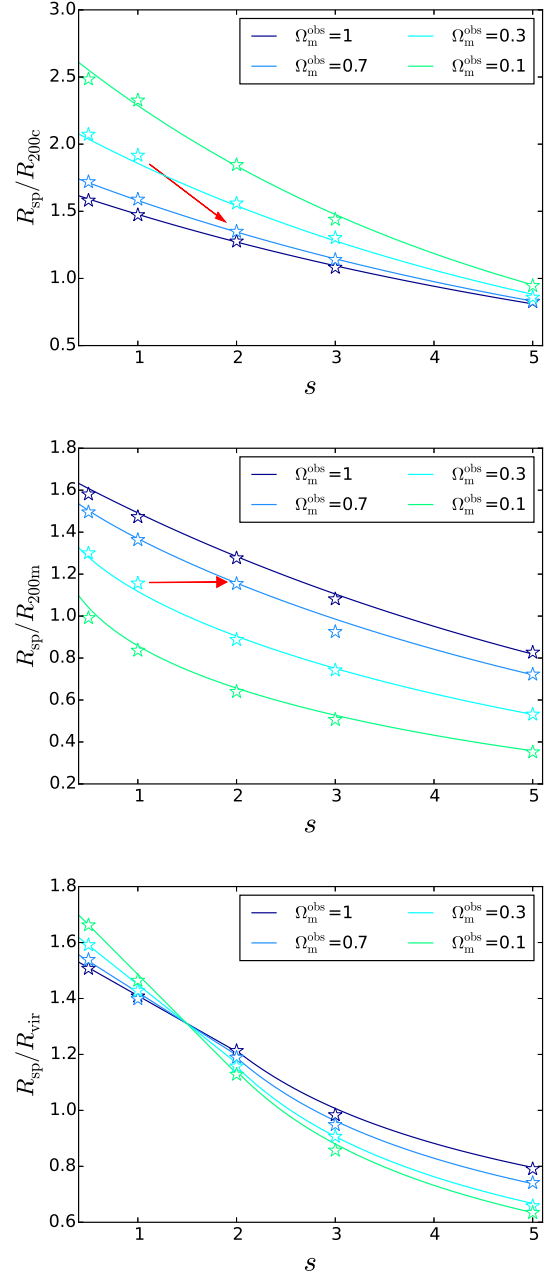


Figure 7. The location of the splashback radius with respect to R_{200c} (upper panel), R_{200m} (middle panel) and R_{vir} (lower panel). Values from numerical integration are shown as the stars. The lines are from fitting formulae Eqs. 3, 4 and 5, respectively. The red arrows in the upper and middle panels demonstrate how the R_{sp}/R_{200c} and R_{sp}/R_{200m} ratios would typically change between halo samples observed at two redshifts. That the orientation of the arrow for R_{sp}/R_{200m} would typically be more horizontal explains why R_{sp} scales better with R_{200m} than R_{200c} (see text for more details).

$$\frac{R_{\text{sp}}}{R_{200m}} = \text{Exp} \left[(0.24 + 0.074 \ln s) \ln \Omega_{\text{m}}^{\text{obs}} + 0.55 - 0.15s \right], \quad (4)$$

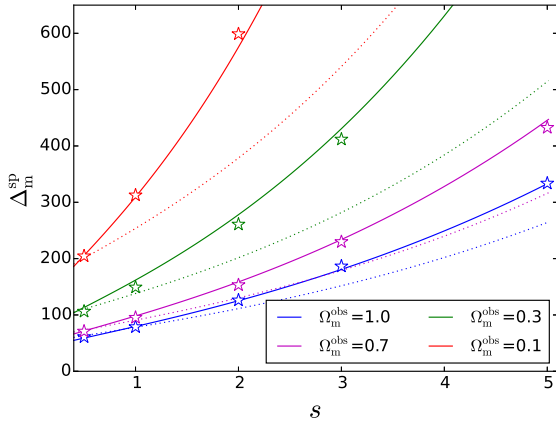


Figure 8. The overdensity at the splashback radius. Solid lines show fitting formula Eq. 7 to our results from numerical integration (stars). In comparison, the Adhikari, Dalal & Chamberlain (2014) fitting formula is shown as the dotted lines.

$$\frac{R_{sp}}{R_{vir}} = \begin{cases} (-0.2 + 0.067 \ln \Omega_m^{obs}) \ln s + 1.6 - 0.1 \ln \Omega_m^{obs} & \text{if } s \leq 2; \\ \text{Exp} \left[(-0.66 + 0.2 \ln \Omega_m^{obs}) \ln s + 0.58 - 0.07 \ln \Omega_m^{obs} \right] & \text{if } s > 2. \end{cases} \quad (5)$$

The locations of R_{200c} , R_{200m} and R_{vir} are determined using the mass profiles, and R_{sp} using the outmost radius where the density diverges in the un-smoothed density profiles. The mean overdensity within R_{vir} at virial radius depends on cosmology as (Bryan & Norman 1998)

$$\Delta_{c,vir}(\Omega_m) = 18\pi^2 + 82(\Omega_m - 1) - 39(\Omega_m - 1)^2 \quad (6)$$

(see also Lacey & Cole 1993; Nakamura & Suto 1997, for other fitting formulae).

For other reference radii e.g. R_{500m} , one can use $M \propto R^\Upsilon$ with Υ given by Eq. (1) as an approximation of the outer mass profile to scale the reference radii to R_{200c} or R_{200m} . For example, $R_{500m}/R_{200m} = (500/200)^{1/(\Upsilon-3)}$. This holds approximately correct as long as the chosen reference radius is large enough that relaxation physics is still sub-dominant compared to accretion.

Fig. 7 shows the numerically integrated results for the locations of the splashback radius in comparison with the fitting formulae. In units of R_{200c} or R_{200m} , the splashback radius also decreases with increasing accretion rate s (Fig. 7), consistent with numerical findings (Diemer & Kravtsov 2014; Lau et al. 2015) and analytical results from Adhikari, Dalal & Chamberlain (2014). We also notice the good agreement on the accretion rate dependence of R_{sp}/R_{200m} between our result and the numerical result of More, Diemer & Kravtsov (2015) (their Fig. 3) within the tested range of mass accretion rates and redshifts, despite of the imperfect match between s and the accretion rate indicator measured from simulations. The dependence on Ω_m^{obs} differs when scaled with R_{200c} or R_{200m} . The ratio R_{sp}/R_{200c} decreases with increasing Ω_m^{obs} at small accretion rate, while saturates to $R_{sp}/R_{200c} \lesssim 1$ at large accretion rate for all Ω_m^{obs} values. In comparison, the ratio R_{sp}/R_{200m} increases with Ω_m^{obs} at all accretion rates (Fig. 7).

Numerical studies (Diemer & Kravtsov 2014; Lau et al. 2015) have found that the splashback radius of halos at different redshifts

align much better with each other when scaled with R_{200m} than R_{200c} . The origin of this intriguing property has not yet been understood. From our results (see e.g. Fig. 7), the alignment of the splashback radius is *not* better with R_{200m} than R_{200c} at a fixed accretion rate for the cosmology and redshift range considered in the simulations ($\Omega_m^{obs} \approx 0.3$ or greater). The apparent better alignment when scaled with R_{200m} is an outcome of correlated increase of Ω_m^{obs} and the average halo mass accretion rate with redshift: the decrease of R_{sp}/R_{200m} with s and the increase with Ω_m^{obs} cancel each other to some extent; on the other hand R_{sp}/R_{200c} decreases with both Ω_m^{obs} and s , which leads to an inevitable decrease of R_{sp}/R_{200c} with redshift (see the red arrows in Fig. 7).

Another way of describing the location of the splashback radius is to look at the mean overdensity within it Δ_m^{sp} . However, this representation is more susceptible to the inner mass profile and thus demands a more careful description of it taking account of the relaxation processes. Therefore, the self-similar solutions are not best represented in terms of Δ_m^{sp} . Nevertheless, we provide a fitting formula to Δ_m^{sp} ,

$$\Delta_m^{sp} := \frac{\langle \rho \rangle (< R_{sp})}{\bar{\rho}} = 33 (\Omega_m^{obs})^{-0.45} \text{Exp} \left[(0.88 - 0.14 \ln \Omega_m^{obs}) s^{0.6} \right], \quad (7)$$

and compare it to the previous work of Adhikari, Dalal & Chamberlain (2014). Our fitting formula (solid lines in Fig. 8) agrees well with that given in Adhikari, Dalal & Chamberlain (2014) (dotted lines) in the limit of small accretion rates. When the accretion rate is large, our results yield larger Δ_m^{sp} especially at low Ω_m^{obs} . The difference arises from the different theoretical approaches of the two methods: while we use the self-similarity ansatz to compute the trajectories of many shells and the mass profile consistently, Adhikari, Dalal & Chamberlain (2014) imposed a more realistic NFW profile of the dark matter halo but computed only the trajectory of one shell without making it consistent with the mass profile. We assess how much of the difference arises from the different mass profile in Appendix. C.

4 SUMMARY AND CONCLUSION

Being dominated by recent accretions rather than by relaxation processes, the outer profile of dark matter halos can be reasonably well-described by one dimensional spherical collapse models. The challenge, however, is to consistently treat the trajectories of dark matter shells and the mass profile of dark matter halos in a Λ CDM universe.

We achieved this by generalising the self-similar spherical collapse model of Fillmore & Goldreich (1984) to a Λ CDM universe. To remedy the loss of strict self-similarity, we simultaneously computed the trajectories of dark matter shells that collapsed at different cosmic times using a simple dimensionless form of the spherical collapse model which reduced the computational effort.

The resulting dark matter profiles depend on two parameters: the mass accretion rate of the dark matter halo, and the matter content of the universe (and thus the redshift). We find that the shape of dark matter profiles are clearly separated into an inner power law profile whose slope depends on the mass accretion rate but not on the redshift, and an accretion region where the profiles depend on both, but can be described easily by the spherical collapse of a single shell to a good approximation. These inner and accretion regions are linked by a sharp transiting region around the splashback radius, where the dark matter density drops abruptly by a factor of $\sim 4 - 5$.

We confirmed, and provided more understanding to previous results on how the splashback radius depends on the accretion rate and the redshift. In particular, the puzzling numerical discovery that the splashback radius R_{sp} scales well with $R_{200\text{m}}$ rather than with the more frequently used $R_{200\text{c}}$ is found to be an outcome of the correlated increase of $\Omega_{\text{m}}^{\text{obs}}$ and the average halo mass accretion rate with redshift and their canceling effects on $R_{\text{sp}}/R_{200\text{m}}$.

New fitting formulae of the splashback radius in various forms are provided. Our results can aid the interpretation of observations of diffuse hot gas and weak gravitational lensing observations in the outskirts of galaxy clusters. We recommend to use $R_{\text{sp}}/R_{200\text{m}}$, which is less sensitive to the shape of mass profiles, as the quantity to link analytical studies to simulations and observations.

ACKNOWLEDGEMENTS

XS thanks Eiichiro Komatsu for carefully reading the manuscript and giving helpful suggestions, as well as Erwin Lau and Surhud More for discussions and comments, and Susmita Adhikari for explaining the details of their method.

REFERENCES

- Adhikari S., Dalal N., Chamberlain R. T., 2014, JCAP, 11, 19
 Bertschinger E., 1985, ApJS, 58, 39
 Binney J., Tremaine S., 2008, Galactic Dynamics: Second Edition. Princeton University Press
 Bryan G. L., Norman M. L., 1998, ApJ, 495, 80
 Correa C. A., Wyithe J. S. B., Schaye J., Duffy A. R., 2015, MNRAS, 450, 1521
 Diemer B., Kravtsov A. V., 2014, ApJ, 789, 1
 Eke V. R., Cole S., Frenk C. S., 1996, MNRAS, 282, 263
 Fillmore J. A., Goldreich P., 1984, ApJ, 281, 1
 Gradshteyn I. S., Ryzhik I. M., 1965, Table of integrals, series and products
 Hahn O., Angulo R. E., 2016, MNRAS, 455, 1115
 Henriksen R. N., Widrow L. M., 1999, MNRAS, 302, 321
 Ichiki K., Takada M., 2012, Phys. Rev. D, 85, 063521
 Lacey C., Cole S., 1993, MNRAS, 262, 627
 Lau E. T., Nagai D., Avestruz C., Nelson K., Vikhlinin A., 2015, ApJ, 806, 68
 Lithwick Y., Dalal N., 2011, ApJ, 734, 100
 MacMillan J. D., Widrow L. M., Henriksen R. N., 2006, ApJ, 653, 43
 Merritt D., Aguilar L. A., 1985, MNRAS, 217, 787
 Mo H., van den Bosch F. C., White S., 2010, Galaxy Formation and Evolution
 More S., Diemer B., Kravtsov A. V., 2015, ApJ, 810, 36
 More S. et al., 2016, preprint (arXiv: 1601.06063)
 Nakamura T. T., Suto Y., 1997, Progress of Theoretical Physics, 97, 49
 Navarro J. F., Frenk C. S., White S. D. M., 1996, ApJ, 462, 563
 Navarro J. F., Frenk C. S., White S. D. M., 1997, ApJ, 490, 493
 Patej A., Loeb A., 2015, preprint (arXiv: 1509.07506)
 Peñarrubia J., 2013, MNRAS, 433, 2576
 Subramanian K., Cen R., Ostriker J. P., 2000, ApJ, 538, 528
 Vogelsberger M., Mohayaee R., White S. D. M., 2011, MNRAS, 414, 3044
 Vogelsberger M., White S. D. M., Mohayaee R., Springel V., 2009, MNRAS, 400, 2174

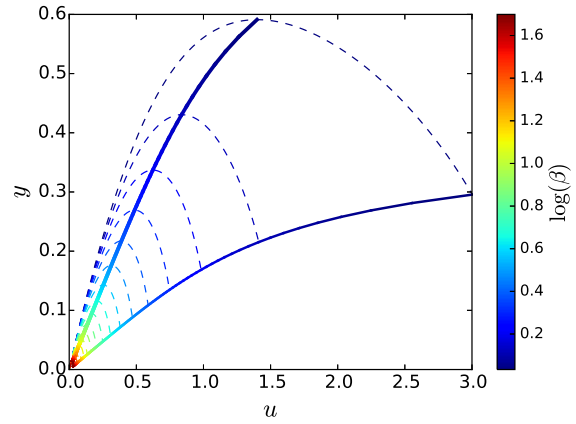


Figure A1. Spherical collapse trajectories (scaled radius y as a function of scaled cosmic scale factor u) in an Λ CDM universe (dashed lines) for shells with different scaled initial overdensities β (shown with different colors). The turn-around locations of the trajectories are marked as the upper solid line, whose analytical expression is given by Eqs. A9 and A12. The locations where the shells collapse to half their turn-around radius are shown as the lower solid line.

APPENDIX A: MINIMALISTIC DIMENSIONLESS FORM OF SPHERICAL COLLAPSE IN A $\Omega_{\text{M}} + \Omega_{\Lambda} = 1$ UNIVERSE

We consider the nonlinear evolution of a spherical region with overdensity $\delta(R_i)$. The evolution of radius R of the shell encompassing mass M shares the same dynamical equation with the background universe (e.g. Mo, van den Bosch & White 2010)

$$\frac{d^2 R}{dt^2} = -\frac{GM}{R^2} + \frac{\Lambda R}{3}, \quad (\text{A1})$$

but has a different energy equation including the effect of its curvature K ,

$$\left(\frac{dR}{dt}\right)^2 = \frac{2GM_i}{R} + \frac{\Lambda R^2}{3} - K. \quad (\text{A2})$$

Here, Λ is the cosmological constant, M_i is the initial mass encompassed by the shell, and $R_i = R(a_i)/a_i$ is the comoving size of the shell at the initial time when the cosmic scale factor $a = a_i$. Since the density fluctuations are small in the early universe, $\delta(R_i) \ll 1$, the mass of the overdense region is $M_i = 4\pi\bar{\rho}_0 R_i^3/3$ to a good approximation, with $\bar{\rho}$ being the mean matter density of the universe, and subscript ‘0’ indicates today ($a = 1$).

Compared to the background universe with $K = 0$, the shell expands more slowly. A shell encompassing a large overdensity finally turns around at a radius R_{ta} and starts to infall towards the center (see trajectories of the shells as dashed lines in Fig. A1). Shell-crossing happens after this turn-around and the energy equation (A2) is no longer valid due to the interactions among different shells.

Even before turn-around, the dynamical behavior of the shell is determined by three parameters:

- the mass / size of the overdense region
- its overdensity with respect to the mean matter density, which determines the curvature of the overdense region when the latter is viewed as a separate universe (e.g. Ichiki & Takada 2012)
- the value of the cosmological constant which sets a typical time scale in the evolution of the universe.

We shall reduce the number of parameters to gain general quantita-

Table A1. Summary of the notations for the variables describing the background cosmology (the first three rows) and the spherical overdense region (the last three rows), both in their original and scaled forms. In the scaled forms, the dimensional physical scales defined by the mass of the initial overdense region M_i , its comoving radius $R_i = R(a_i)/a_i$ and the mean overdensity of the universe at redshift zero ρ_0 are taken out of the cosmological constant, time, the curvature and the radius of the overdense region; and the cosmology as described by the scaled cosmological constant is taken out of the cosmic scale factor, time, the overdensity and the radius of the overdense region.

	Original	Scaled
Cosmological constant	Λ	$w = \Lambda R_i^3 / (6GM_i) = \Omega_{m0}^{-1} - 1$
Cosmic scale factor	a	$u = w^{1/3} a$
Time	t	$I = (8\pi G \rho_0 w / 3)^{1/2} t$
Curvature	K	$\kappa = KR_i / (2GM_i)$
Overdensity	δ	$\beta = \kappa / \kappa_{\min}$ with $\kappa_{\min} = 3w^{1/3} / 2^{2/3}$
Radius	R	$y = w^{1/3} R / R_i$

tive properties of the spherical collapse. Eke, Cole & Frenk (1996) have presented a dimensionless form of the spherical collapse equations with two parameters: scaled Λ and K defined as (see Table. A for a summary of the notations)

$$w := \Lambda R_i^3 / 6GM_i = \Omega_{m0}^{-1} - 1 \rightarrow \begin{cases} \infty & \text{for } \Omega_{m0} \rightarrow 0 \\ 0 & \text{for } \Omega_{m0} \rightarrow 1 \text{ (EdS universe)} \\ 1 & \text{when } \Omega_{m0} = \Omega_{\Lambda 0}, \end{cases} \quad (\text{A3})$$

$$\kappa := KR_i / 2GM_i \propto \delta. \quad (\text{A4})$$

They also showed that, in a universe with a non-zero cosmological constant ($w > 0$), a minimum initial overdensity which corresponds to $\kappa_{\min} = 3w^{1/3} / 2^{2/3}$ is required for a shell to collapse.

We use this to define a new parameter $\beta := \kappa / \kappa_{\min}$ to describe the overdensity of the shell. At the same time, we further scale out the cosmology (' w ') dependencies in the radius and time variables:

$$y := w^{1/3} R / R_i, \quad (\text{A5})$$

$$I := \left(\frac{8\pi G \bar{\rho}_0 w}{3} \right)^{1/2} t = (1 - \Omega_{m0})^{1/2} H_0 t,$$

with H_0 being the Hubble constant. The scaled time I has a simple analytical relation with the scaled cosmic scale factor $u := w^{1/3} a$,

$$I = \frac{2}{3} \operatorname{arcsinh}(u^{3/2}). \quad (\text{A6})$$

With these definitions, $u = (1 - \Omega_m)^{1/3} / \Omega_m^{1/3}$ reflects the ratio of dark energy and dark matter at that time, $y \approx u$ in the early times when the overdensity is small and the overdense region expand with nearly the same speed as that of the background universe (Fig. A1).

Written in terms of these scaled parameters, the dynamical equation (A1) and the energy equation (A2) become

$$\frac{d^2 y}{dI^2} = -\frac{M}{2M_i} \frac{1}{y^2} + y, \quad (\text{A7})$$

and

$$\left(\frac{dy}{dI} \right)^2 = y^{-1} + y^2 - 3\beta/2^{2/3} = (y - y^*)(y + y^* - 1/y/y^*) \quad (\text{A8})$$

with y^* being the scaled turn-around radius of the shell ². Again, Eq. (A8) no longer holds after shell-crossing, while Eq. (A7) still does as long as the actual enclosed mass $M(< R)$ is used.

The trajectories of the shells in the absence of shell-crossing until they reach half of their turn-around radius ('hrt'a') are shown in Fig. A1. Now, a shell is characterised solely by its scaled overdensity β . The physical scale of the shell is only important in the shell-crossing region. Cosmology dependence is removed from the dynamical and energy equations. Different cosmologies correspond to different values of u_0 and I_0 , or u_{obs} and I_{obs} in a more general sense when we label a universe with its Ω_{m0}^{obs} value at the time of observation irrespective of the corresponding redshift. In particular, an EdS universe corresponds to $u_{\text{obs}} \ll 1$ and $I_{\text{obs}} \ll 1$, and the shells collapsed before this time must have $\beta \gg 1$ (Fig. A1). A Λ CDM universe with $\Omega_m = 0.3$ has $u_{\text{obs}} = (0.3^{-1} - 1)^{1/3} \approx 1.326$.

Due to the simple form of the scaled spherical collapse equation in the single-stream regime (Eq. A8), useful analytical relations can be derived among the variables (see Appendix. A1). These relations also enable easy determination of initial conditions for the numerical integration of the dynamical equation in the shell-crossing regime.

A1 Analytical relations in the single stream regime of spherical collapse

From the scaled spherical collapse equation Eq. (A8), we can derive an analytical expression for the scaled turn-around radius y^* as a function of the scaled overdensity β ,

$$y^* = 2^{2/3} \beta^{1/2} \sin \left(\frac{1}{3} \sin^{-1} \left(\beta^{-3/2} \right) \right), \quad (\text{A9})$$

or reversely,

$$\beta = \frac{2^{2/3}}{3} (y^{*-1} + y^{*2}). \quad (\text{A10})$$

For $\beta \gg 1$, $y^* \leq 2^{-1/3}$, i.e. there exists a maximum radius for collapsing regions. In the far future when dark energy completely dominates the energy content of the universe, all halos will have a truncation radius beyond which matter can no longer fall onto them (cf. Subramanian, Cen & Ostriker 2000).

Until turn-around, the relation between time and radius is monotonous, which allows us to express the scaled time as a function of the scaled radius,

$$I = \int_0^{y/y^*} \frac{\sqrt{x} dx}{\sqrt{(x-1)(x^2 + x - 1/y/y^3)}}. \quad (\text{A11})$$

This form can be written in terms of elliptical integrals. In particular, the integral to $y = y^*$ can be expressed as the sum of two complete elliptic integrals Π (3rd kind) and K (1st kind),

$$I^* = \frac{1 + \sqrt{1 + 4A}}{\sqrt{A - 1/2 + \sqrt{1 + 4A/2}}} [\Pi(B, C) - K(C)], \quad (\text{A12})$$

with $A \equiv 1/y^{*3}$, $B \equiv 2/(3 + \sqrt{1 + 4A})$, and $C \equiv \sqrt{1 + 4A}/(A - 1/2 + \sqrt{1 + 4A/2})$ (see Gradshteyn & Ryzhik 1965 3.148.4).

² We will use superscript '*' to indicate the quantities at the turn-around radius of the shell. In contrast, the quantities at the turn-around radius at the time of observation (i.e. $t^* = t^{\text{obs}}$) will be indicated with subscript 'ta'.

The ratio of the average density within a shell and the mean matter density of the universe is given by the simple relation

$$\Delta_m := \frac{\langle \rho(< y) \rangle}{\bar{\rho}} = \frac{u^3}{y^3} \quad (\text{A13})$$

before shell crossing. After shell-crossing, it should be modified to

$$\Delta_m = \frac{u^3}{y^3} \frac{M(< y)}{M_i}. \quad (\text{A14})$$

In the limit of an EdS universe, i.e. $\beta \rightarrow \infty$, we have

$$\begin{aligned} y^* &\rightarrow 2^{2/3} (3\beta)^{-1}, \\ I(y, \beta) &\rightarrow y^{*3/2} \left[\arcsin \sqrt{y/y^*} - \sqrt{(1 - y/y^*)y/y^*} \right], \\ I^* &\rightarrow \pi (3\beta)^{-3/2}, \\ y^{*3/2}/I^* &\rightarrow 2/\pi, \\ \Delta_m^* &= \frac{u^{*3}}{y^{*3}} \rightarrow \left[\frac{\sinh^{2/3} (3\pi (3\beta)^{-3/2}/2)}{2^{2/3} (3\beta)^{-1}} \right]^3 \rightarrow 9\pi^2/16 \approx 5.55. \end{aligned} \quad (\text{A15})$$

The last expression on the mean overdensity within the turn-around radius Δ_m^* reproduces the classical result of Lacey & Cole (1993). When generalized to a Λ CDM universe, Δ_m^* depends on Ω_m ,

$$\begin{aligned} \Delta_m^* &\approx \frac{9\pi^2}{16} + u_{\text{obs}}^2 + 2u_{\text{obs}}^3 \\ &= \frac{9\pi^2}{16} + \left(\frac{1 - \Omega_m^{\text{obs}}}{\Omega_m^{\text{obs}}} \right)^{2/3} + 2 \frac{1 - \Omega_m^{\text{obs}}}{\Omega_m^{\text{obs}}}, \end{aligned} \quad (\text{A16})$$

with the approximation precise to within 3% for any value of u_{obs} or Ω_m^{obs} .

A2 Dark matter density profile in the single-stream region

With the dynamics of infall described by Eq. (A8), the dark matter density profile in the single-stream region is fully specified when the physical scales of the dark matter shells are given, e.g., by the mass accretion rate of the central halo. Labeling the dark matter shells by their overdensity parameter β , the density at the location of the shell at epoch u is

$$\begin{aligned} \rho(u, \beta) &= \frac{\partial \ln M}{\partial \ln R} \frac{M}{4\pi R^3} = \bar{\rho}(u) \Delta_m(u, \beta) \frac{\partial \ln R_i}{\partial \ln R} \\ &= \bar{\rho}(u) \frac{u^3}{y^3(u, \beta)} \left[1 + \frac{3}{s} \left(\frac{d \ln u_{\text{hrt}}(\beta)}{d\beta} \right)^{-1} \frac{\partial \ln y}{\partial \beta} \right]^{-1}, \end{aligned} \quad (\text{A17})$$

whereas its radial location is

$$R(u, \beta) = R_i w^{-1/3} y = \left(\frac{3M_{\text{vir}}(u)}{4\pi \bar{\rho}(u)} \right)^{1/3} \left(\frac{u_{\text{hrt}}(\beta)}{u} \right)^{3/s} \frac{y(u, \beta)}{u}. \quad (\text{A18})$$

They can be easily generalised to other parametrised forms of mass accretion history.

APPENDIX B: SPLASHBACK RADIUS IN AN EDS UNIVERSE

As shown by Fillmore & Goldreich (1984), in an EdS universe, for a small accretion rate $s \leq 3/2$, the gravitational potential is static; for $s \geq 3/2$, the potential grows, the orbit contracts, and the amplitude of oscillation decays with time. Namely, since the turn-around radius and the mass enclosed grow in an EdS universe

as $R_{\text{ta}}(I)/R^* = (I/I^*)^{2/3+2s/9}$ and $M_{\text{ta}}(t)/M^* = (I/I^*)^{2s/3}$ (Fillmore & Goldreich 1984, Eqs. 18 and 19),

$$\frac{M(R, t)}{M^*} = \left(\frac{R}{R^*} \right)^{\Upsilon} \left(\frac{R^*}{R_{\text{ta}}} \right)^{\Upsilon} \frac{M_{\text{ta}}}{M^*} = \left(\frac{R}{R^*} \right)^{\Upsilon} \left(\frac{I}{I^*} \right)^{\alpha} \quad (\text{B1})$$

with

$$\alpha = -2\Upsilon/3 - 2\Upsilon s/9 + 2s/3 = \begin{cases} 0 & \text{if } s \leq 3/2 \\ 4s/9 - 2/3 > 0 & \text{if } s \geq 3/2. \end{cases}$$

With these, the dynamical equation describing the oscillation becomes

$$\frac{d^2 R}{dI^2} = -\frac{1}{2w} \left(\frac{I}{I^*} \right)^{\alpha} \frac{R_i^3}{R^{*\Upsilon}} R^{\Upsilon-2}. \quad (\text{B2})$$

For time-independent gravitational potentials (when $s \leq 3/2$), Eq. (B2) does not have explicit time-dependence, and represents an oscillator with a constant amplitude $R_{\text{sp}} = R^*$ and period. Thus, $I_{\text{sp}} \approx 3I^*$, and the $R_{\text{sp}}/R_{\text{ta}}$ ratio reflects only the growth of the turnaround radius with time,

$$\frac{R_{\text{sp}}}{R_{\text{ta}}} = \frac{R^*}{R_{\text{ta}}} = \left(\frac{I_{\text{sp}}}{I^*} \right)^{-2/3-2s/9} \approx 3^{-2/3-2s/9}. \quad (\text{B3})$$

This relation is precise in the limit of $s \rightarrow 0$.

For time-dependent gravitational potentials (when $s > 3/2$), some conserved quantity is usually exploited to describe the amplitude and period change in the oscillator. In the limit of slow mass accretion, the radial action of the orbit is conserved (Binney & Tremaine 2008) even when the gravitational potential grows with time. More generally, a canonical transformation of coordinates can be constructed that removes the explicit time-dependence from the Hamiltonian of the oscillating shell (Peñarrubia 2013). In our case of time varying power-law potentials with mass profile slope of $\Upsilon = 1$ (Eq. 1), the transformation is approximately $R' = (I/I^*)^{\alpha/2} R$ and $d\tau = (I/I^*)^{\alpha} dI$. To linear order, the dynamical equation expressed in the transformed quantities

$$\frac{d^2 R'}{d\tau^2} = -\frac{1}{2w} \frac{R_i'^3}{R'^{\Upsilon}} R'^{-1} \quad (\text{B4})$$

represents an oscillator with a period of

$$\tau_p = 4\sqrt{\pi} \sqrt{w} \frac{R'^{s/3/2}}{R_i'^{s/3/2}} = 4\sqrt{\pi} y^{*3/2}, \quad (\text{B5})$$

and a time-independent amplitude, i.e. $R'_{\text{sp}} = R'^*$. Transforming back into the original coordinates, $R_{\text{sp}}/R^* = (I_{\text{sp}}/I^*)^{-\alpha/2}$. Therefore,

$$\frac{R_{\text{sp}}}{R_{\text{ta}}} = \frac{R_{\text{sp}}}{R^*} \frac{R^*}{R_{\text{ta}}} = (I_{\text{sp}}/I^*)^{-2/3-2s/9-\alpha/2} = (I_{\text{sp}}/I^*)^{-\alpha-1}. \quad (\text{B6})$$

A shell moving from its turnaround to splashback location completes half an oscillation, thus

$$\tau_{\text{sp}} - \tau^* = (I_{\text{sp}}^{\alpha+1} - I^{*\alpha+1})/(\alpha+1)/I^{*\alpha} = \tau_p/2, \quad (\text{B7})$$

which, together with Eq. (B5), gives

$$I_{\text{sp}}^{\alpha+1} = I^{*\alpha+1} + 2(\alpha+1)\sqrt{\pi} y^{*3/2} I^{*\alpha}. \quad (\text{B8})$$

Inserting this into Eq. (B6) finally gives

$$\frac{R_{\text{sp}}}{R_{\text{ta}}} = \left[1 + 2(\alpha+1)\sqrt{\pi} y^{*3/2}/I^* \right]^{-1} = \left[1 + 4(4s/9 + 1/3)/\sqrt{\pi} \right]^{-1}. \quad (\text{B9})$$

Note that this relation is derived under the approximation of a

power-law mass profile which does not capture the full profile shape in the halo outskirts. In addition, in the limit of extremely high mass accretion rates, Eq. B9 will fail from neglecting the non-linear corrections in the coordinate transformations.

Thus, in summary, we have obtained two analytical approximations for the value of $R_{\text{sp}}/R_{\text{ta}}$ in an EdS universe as a function of the accretion rate s (Eqs. B3 and B9) suited for $s \leq 3/2$ and $s \geq 3/2$ respectively. As shown by Fig. 5, they describe the numerically integrated values rather well for the tested range of $s \leq 5$.

APPENDIX C: EFFECT OF MASS PROFILE ON THE SPLASHBACK POSITION

How do different mass profiles affect the position of splashback? We assess this by generalising the Adhikari, Dalal & Chamberlain (2014) method: tracing the trajectory of one dark matter shell through a growing dark matter halo with an NFW profile, to dark matter halos with different mass profiles (upper panel of Fig. C1). The mass profiles considered are constructed to have the same value and slope at R_{hrta} , but different inner slopes. The mass profile slope at R_{hrta} is derived from the Fillmore & Goldreich formula (Eq. 1) and thus is similar to that of our self-similar solutions³.

The resulting Δ_m^{sp} as a function of the mass accretion rate s and the redshift, or more precisely, the matter content of the universe at the time of observation Ω_m^{obs} is shown as lines with different line-styles in the middle panel of Fig. C1. The difference between them presents the degree of influence of different mass profiles, while the difference between the solid lines and the stars (our self-similar result) presents that of the different theoretical assumptions of Adhikari et al. and our self-similar approach. Both effects matter to similar degree.

Different mass profiles affect Δ_m^{sp} not only through different gravitational dynamics they lead to, but also simply from the radius-overdensity conversion. To reduce the second effect, we present the comparison again in terms of $R_{\text{sp}}/R_{200\text{m}}$ (lower panel of Fig. C1). In terms of $R_{\text{sp}}/R_{200\text{m}}$, the splashback locations predicted with different mass profiles differ much less. Therefore, we recommend to use this representation to compare with simulations and observations. In this representation, the result from the self-similar solution and that from the Adhikari et al. method agree to better than 10% for all mass accretion rates examined when $\Omega_m^{\text{obs}} \geq 0.3$.

³ However, this is different from the original Adhikari, Dalal & Chamberlain (2014) choice, which uses a mass profile slope of $3s/(s+3)$ without the saturation at $s \geq 3/2$. To differentiate the two, we refer to our reproduced result as ‘result from the Adhikari et al. method’. Matching the mass profile slope of $3s/(s+3)$ without a saturation to an NFW halo would lead to unrealistically small concentration parameters at relatively large mass accretion rates, e.g. $c < 1$ for $s > 2.28$, and significantly smaller Δ_m^{sp} there.

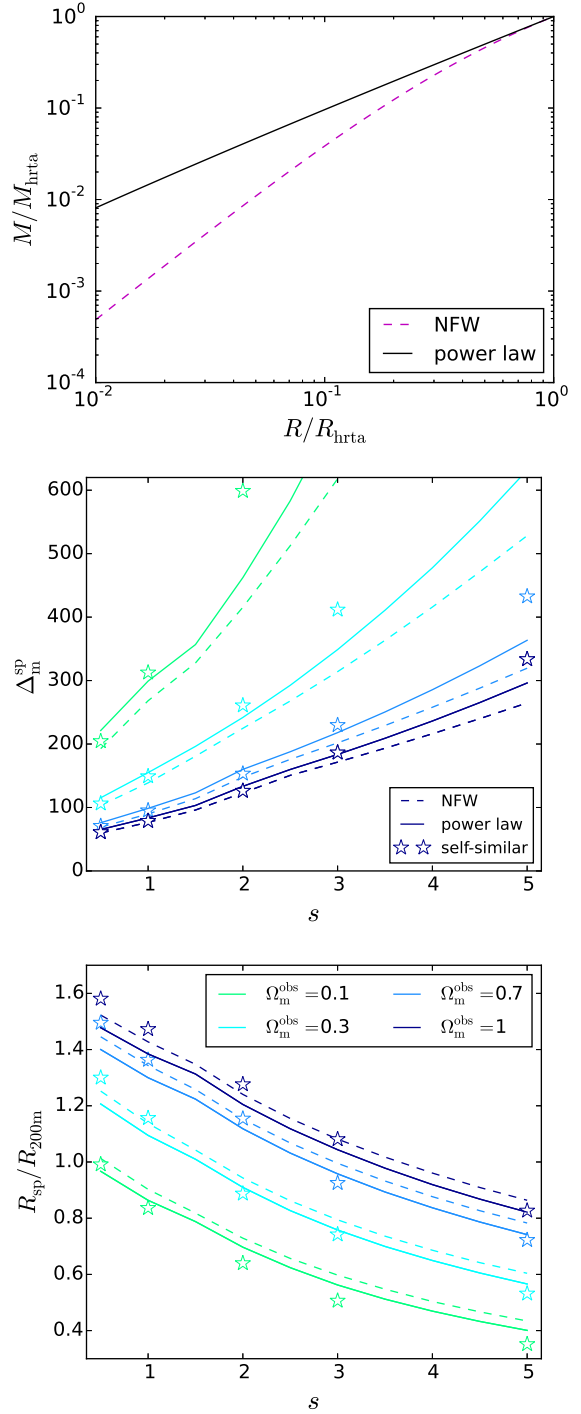


Figure C1. *Upper panel:* Different mass profiles used for computing the splashback radius with the Adhikari et al. method. ‘NFW’ presents the profile used in Adhikari et al. paper for mass accretion rates $s = 1.5$, and ‘power law’ is the corresponding profile with power-law index given by Eq. (1). *Middle panel:* The overdensity at the splashback radius. The stars show the results from the self-similar model as presented in Fig. 8. The dashed lines show reproduced results of Adhikari et al., and the solid lines show results using the Adhikari et al. method but with power law mass profiles. Different Ω_m^{obs} values (0.1, 0.3, 0.7, 1) are indicated by different colors, from light green to dark blue, respectively. *Lower panel:* The splashback radius in terms of $R_{\text{sp}}/R_{200\text{m}}$. Labels are the same as the middle panel.